SYNTHESIS OF A NANOSTRUCTURED Al-Cu POWDER ALLOY WITH ADDITIONS OF TiC PARTICLES BY MECHANICAL ALLOYING AND BALL MILLING – MATHEMATICAL MODELLING OF MICROSTRUCTURE

S. GAONA-JIMENEZ[a], R. A. RODRÍGUEZ-DÍAZ[a*], A. SEDANO[b], J. PORCAYO-CALDERON[b], A. M. OCAMPO[b], S. SERNA-BARQUERA[b], J. O. OLARTE-CORTES[a], J. A. JUÁREZ-ISLAS[c].

[a]*Polytechnic University of Morelos State, Boulevard Cuauhnahuac 566, Col. Lomas del Texcal, 62574, Jiutepec, Morelos, México*

[b]*Research Center in Engineering and Applied Sciences, UAEM, Av. Universidad 1001, Col, Chamilpa, Cuernavaca, Morelos, México*

[c]*Materials Research Institute – National University Autonomous of Mexico UNAM, circuito exterior S/N, Ciudad Universitaria, C. P. 04510, Cd. de México, México*

In this work, a composite material of nanostructured Al based matrix and reinforced with TiC was prepared by two variants of milling: mechanical alloying and ball milling. During the mechanical alloying, a solid solution of Copper dissolved in Aluminum matrix (Al-α) was prepared from a stoichiometric mixture of high purity powders of Cu and Al. In the course of the ball milling stage, the powder mixture composed by the TiC phase was mixed with the solid solution (Al-α). This mixture was mechanically milled under conditions of low energy. In accordance with the X-ray diffraction analysis, a solid solution of Cu in Al was produced at the tenth hour of milling. The crystallite size pertaining to the solid solution of Cu in Al (α-Al), decreased from 55 to 33 nm as the milling time elapsed from 2.5 to 20 h. During the mechanical milling stage, the powder mixture composed by the solid solution Al-α together with TiC phase did not undergo a mechanochemical reaction that could give place to the formation of second phases. Besides, during ball milling process, an additional reduction of crystallite size of Al-α phase was revealed, this behavior is because ceramic TiC particles acted as milling media. Besides, Mathematical descriptive models were fitted to the variation of the microstructural features as a function of processing time. Such microstructural characteristics are: particle size, crystallite size, lattice parameter and dislocation density.

(Received January 23, 2017; Accepted May 22, 2017)

Keywords: Nanostructured Alloy, Nanocomposite, Al Alloy, Mechanical Alloying, Mechanical Milling, Solid Solution

1. Introduction

During various decades the nanostructured or nanocrystalline materials have been synthesized by various production methods and techniques which are mentioned as follows: physical/chemical vapor condensation, electrodeposition [1], gas-phase synthesis (e.g., inert gas condensation [2]), spray pyrolysis, flame synthesis, high-temperature evaporation and, plasma synthesis techniques. It is worth not to disregard the following methods: wet chemical processes including sol-gel, chemical reduction, and biological methods [3].

Among the production methods, which involve breaking down the bulk solid material in particles with nanometer-sized grains; the mechanical processes can be mentioned, i. e., mechanical alloying, high-energy ball milling [4,5], high pressure torsion [6,7], equal channel angular pressing [8,6] and, accumulative roll bonding [9].

Ball or mechanical milling is a widely used technique for the elaboration of nanostructured metallic powders [4,5]. The reduction of grain-size in the powder mixture is achieved by the

*Corresponding author: rdiaz.unam@gmail.com

repeated fracturing and rewelding of powder particles in a highly energetic ball mill. In this case, both processes are originated by the repeated collisions occurring within the mill, which involves the elements: ball-particle-ball.

This technology was formerly developed by Benjamin [10] for the elaboration of Ni-based Oxide Dispersion Strengthened (ODS) super alloys since about 4 decades ago.

Various kinds of nanocomposites have also been synthesized by ball milling or mechanical alloying (MA). In addition, a thermal treatment of crystallization applied to amorphous phases obtained by a combination of Mechanical alloying and Mechanical Milling can give place to the formation of nanocomposites [11].

A significant advantage of the nanocomposites is the prevention or reduction of growth of crystallites or grains, when these materials are subjected to high temperatures once the composite is in consolidated state [12].

Nanocomposites have also been synthetized by mechanochemical reactions induced by mechanical milling [13,14]. A relevant characteristic of these phases and compounds produced by solid state mechanochemical reactions, is that they possess nanometric sized grains, and consequently, these phases exhibit enhanced properties and better performance as compared with the phases and compounds with coarse sized grains.

Aluminum matrix composites provide a combination of higher stiffness-to-density ratio, enhanced elevated temperature properties and improved tribological performance as compared with the conventional Al alloys. These composites can be applied in the construction, aerospace and transportation industrial sectors.

The composite materials, which possess a uniform dispersion of reinforcing particles in the range of 10 nm to 1μm are denominated as "nanocomposites". The mechanical behaviour of the nanometric dispersion strengthened Al matrix composites is much better than Aluminum Matrix Composites reinforced behavior with micrometric particles with a similar volume fraction of the reinforcing phase. However, an homogeneous dispersion of reinforcing phases is essential in order to enhance the mechanical properties of the composites [15].

MA technique is capable of producing composite powders with uniform dispersion of nanoparticles within the matrix alloy. Some examples of the nanocomposite systems that have been synthesized by MA are: Cu/Fe_3C [16], Mg/carbon nanotube [17], Mg/Cr_2O_3 [18], Zn/Al_2O_3 [19], Ni/AlN [20] and Co/Al_2O_3 [21].

Therefore, the purpose of this work is to report the elaboration of a particulate nanostructured Al matrix nanocomposite modified with TiC by mechanical alloying, combined with mechanical milling processes.

2. Materials and methods

Metallic powders of Cu and Al (99.9 % purity) were blended and mixed in a mortar in stoichiometric ratio to yield the composition of Al-3Cu (wt. %). The powder mixture was poured in a hardened steel vial with balls of stainless steel. Analytical grade methyl alcohol, as Process Control Agent (PCA), was added in a ratio of 0.003 ml/g of the powder mixture. Powder mixture was put inside the hardened steel vial under an argon atmosphere and sealed with a cap. Then, the mixture was subjected to mechanical milling in a planetary mill at 500 RPM and different milling times: 2.5, 5, 7.5, 10, 15 and 20 h. During the ball milling process, a balls-to-powder weight ratio of 10: 1 was used.

After 20 h of milling process, at this milling time the nanostructured Al-3Cu alloy was formed, TiC was added. Ratios used were 10 and 15 (% vol). Metallic alloy and ceramic particles were blended in a mortar. Later, the mixture of phases were put inside the vials with the balls inside and were sealed under the same inert atmosphere. Then, the mixture was ball milled for 8 h at 200 RPM.

During the mechanical milling process the evolution of morphology, particle size variation, distribution of the ceramic phase, and the chemical homogenization of the powder mixture were observed in a scanning electron microscope (SEM) mark Estereoscan 440 connected to a Si detector with window of Be (mark Oxford Pentafel) with a resolution of 163 eV which was

attached to a software of Energy Dispersive Spectroscopy (EDS). This technique was also applied to carry out punctual chemical analysis and X-Ray mappings in the un-milled and processed samples, in order to determine the chemical composition and phase's distribution while the milling time had elapsed.

X-Ray Diffraction technique was utilized to reveal and identify the crystalline structure of the metallic and ceramic phases formed during milling, also to determine the size of the nanometric grains and reticular constants from X-ray Diffraction peaks. This microstructural analysis was carried out in a Siemens Diffractometer D500 using a voltage of 30 kV, and a current of 20 mA. The samples were scanned with a filter of CuKα radiation with wavelength of $\lambda = 1.5418$ Å and using a step of 0.020°/0.6 sec., in a range of 30° to 100°.

3. Results and discussion

3.1. Microstructural analysis of the Al, Cu and Al-Cu powder mixture

Fig. 1 exhibits morphology of the elemental powders in the un-milled condition which corresponds to Al, Cu and TiC in a respective way. Figure 1 a) displays spherical particles of Al (with a mean particle size of 3.8 microns). Figure 1 b) shows dendritic-shaped Cu particles with an average particle size of 75 microns. In addition, figure 1 c) shows TiC particles of an irregular morphology with an average size of particles of 5.6 microns.

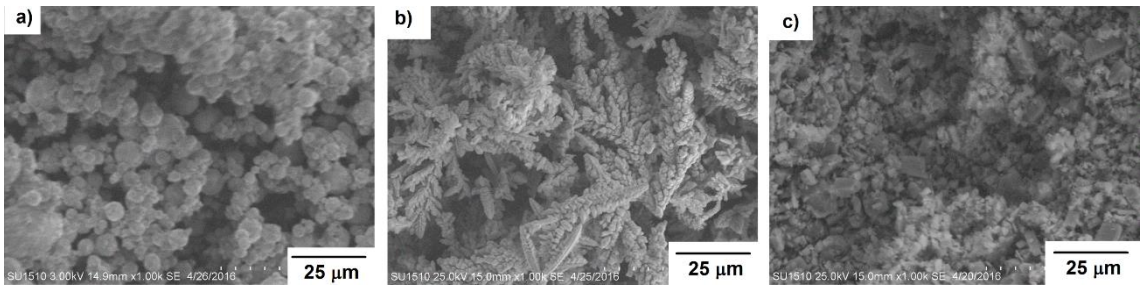

Fig. 1. Secondary electron micrographs of powder particles corresponding to a) Al, b) Cu and c) TiC.

Fig. 2 displays the variation of particle morphology and size. This illustration shows that the particle size diminished as the milling time had elapsed from 2.5 to 20 h. Also, it can be observed that some of the particles for the sample milled during 2.5 h adopted a flake morphology; however, while the milling time had advanced, the morphology of particles turned equiaxial and irregular. Besides, the minimum particle size observed corresponded to the specimen milled during 20 h.

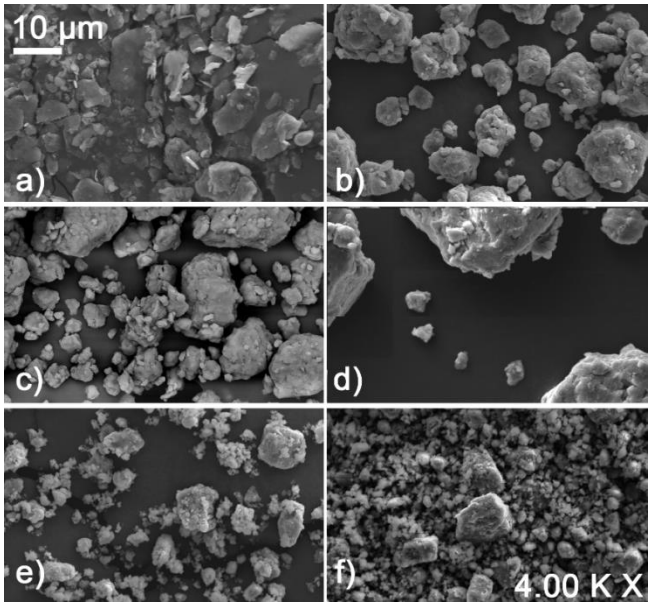

Fig. 2. Microstructural variation of the Al-Cu powders in function of the milling time. (a) 2.5 h, (b) 5 h, (c) 7.5 h, (d) 10 h, (e) 15 h and (f) 20h. (All these micrographs were obtained at the same magnification and scale)

Particle size as a function of milling time (Figure 3 a) and table 1) shows a decrease in average size (from 2.15 to 0.85 microns) and a narrowing of distribution as the milling time increases, see Table 1. The decrease of average particle size is related to the predominance of the fracture processes, which take place under established conditions of mechanical alloying [22]. After long milling times, an equilibrium between cold welding and fracture processes is achieved [23,24], this is related to the slight diminution of particle size after tenth hour of milling, just as is observed in Figure 3 a).

Some mathematical fitting models were adjusted to the data corresponding to the variation of particle size as a function of process time. The best quality for particle size variable was of 98.23%, through the allometric function displayed in equation 1 as follows:

$$P_z = 3.1074t^{-0.41548} \quad (1)$$

In equation 1, "P_z" represents the particle size and "t" is the milling time.

The allometric function adjustment to the data of particle size is displayed in figure 3 a). In this case, the residuals are independent and unbiased. Fisher-Testing which the probability P(Fvalue>Ftable) = 2.10864×10^{-6} is statistically significant (see Fig. 3 b)).

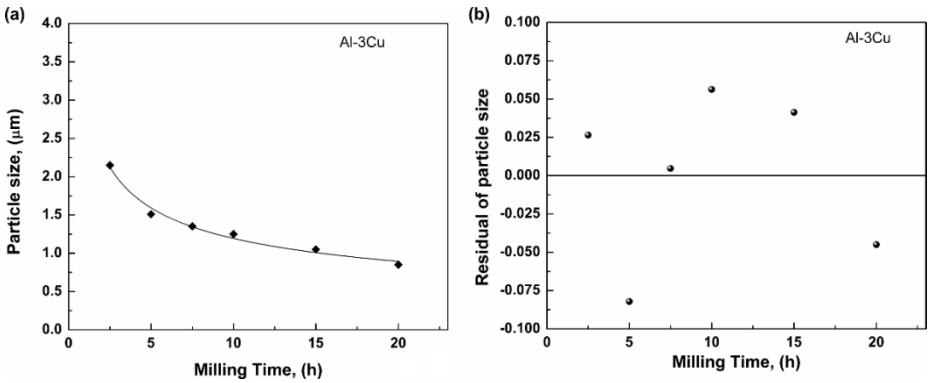

Fig. 3. Variation of the particle size of the powder mixture of Al-3Cu (wt. %) as a function of the milling time, b) Residuals plot of particle size

Table 1. Particle size (μm)

Time (h)	Average	Minimum	Maximum
2.5	2.15	0.85	3.95
5	1.51	0.65	2.30
7.5	1.35	0.40	2.35
10	1.25	0.35	2.25
15	1.05	0.60	1.55
20	0.85	0.45	1.35

3.2. Microstructural characterization by X-ray Diffraction technique of Al-Cu powder mixture

Fig. 4 exhibits the X-ray diffraction profiles of Al-3Cu powders mixture which was subjected to ball milling at different processing times.

Fig. 4 (a) shows the X-Ray Diffraction spectrum of the initial mixture of powders (Al-Cu). According spectrum, the highest peaks of Al and Cu correspond to the reflections produced by the (111) crystallographic planes. From 0 to 7.5 h of milling time, continuous solubilization of Cu in Al took place, since this phenomenon is associated to the continuous decrement of the intensity of the X-Ray Diffraction peaks of Cu. It can be observed that the highest intensity peak of Cu vanished at 10th hour of processing, this behaviour indicates that a complete solubilization of Cu into Al had been achieved at this stage of milling

Although, for an exhaustive characterization of solid solubility in metal powders it is necessary to complement the X-Ray Diffraction technique with Transmission Electron Microscopy (TEM). Only diffraction peaks associated to solid solution of Cu in Al labeled as α-Al can be observed after 10^{th} h of ball milling process.

It can be observed that width of the peaks at half its heights augmented continuously while the milling time had elapsed. This comportment is evidently related with a diminution of the nanometric grains and, also to an increment of the lattice strain or lattice distortion. Usually, there are two typical approaches to determine crystallite size, the first one employs the Scherrer equation [25] and the second one involves Williamson-Hall method application in which the nanometric grains are determined by an equation that includes the crystallite size and the lattice strain [26].

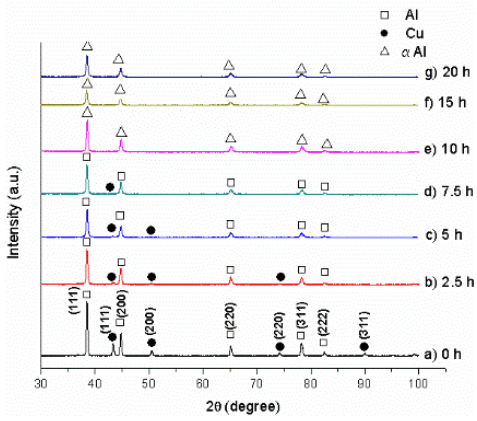

Fig. 4. X-ray Diffraction patterns of Al-Cu powder mixture milled at 500 RPM at various times: a) 0 h, b) 2.5 h, c) 5 h, d) 7.5, e) 10 h, f) 15 h and g) 20 h

In Fig. 5 a), the dependence of crystallite size as a function of processing time is presented. In this illustration is evident that crystallite size exhibits a tendency to decrease in a parallel way while milling process advanced.

In this case, crystallite size together with lattice strain were computed from the Williamson-Hall method [27]. Once crystallite sizes were computed, the mean value of crystallite size was determined. Figure 5 shows a significant decrease of nanosized grains from about 58 to 33 nm when powder mixture was milled from 2.5 to 20 h, respectively. However, from 5 h to 7.5 h of processing, crystallite size increased slightly for about 2.5 nm and after 7.5 h of milling, the size of nanometric grains diminished again.

Crystallite size reduction can be explained in terms of a deformation mechanism that occurs within the nanometric grains. Typically, plastic deformation progresses by slip and twinning at low and intermediate strain rates. However, at high strain rates, the development of shear bands, which are constituted by a dense network of dislocations, becomes the prevalent deformation mechanism [28]. Local shear instability of the crystalline lattice may be caused by material inhomogeneities and could possibly be enhanced by thermoplastic instabilities due to non-uniform heating in certain zones of material during deformation process. In the initial stage of ball-milling process, the average atomic level strain rises due to the continuous increment of dislocation density. When certain level of dislocation density is reached, within these heavily strained regions, the crystal decomposes into subgrains which are initially separated by low-angle grain boundaries. During the progress of ball milling, deformation take place in shear bands located in previously unstrained regions of the material.

Size of the subgrains in the current band is further decreased to the final nano-metric grain size and, relative crystallographic orientation of the subgrains with respect to each other finally acquire complete randomness.

Figure 5 also shows the variation of the lattice strain as the milling process had advanced. This plot shows a drastic increase of lattice strain during the milling time interval from 2.5 to 5 h, this behaviour could be ascribed to an accelerated production of crystallographic defects which were caused by severe plastic deformation induced by the mechanical energy provided by milling media. However, lattice strain diminished drastically as the milling time had elapsed from 5 to 10 hours of process, this behavior is related to a recovery process that typically occurs after plastic deformation with a subsequent temperature rise. It is worth noting that during recovery process, an annihilation of crystal defects occurs. In this case, crystallite size and strain effects acting simultaneously produce the broadening of a profile. In permanently deformed metals and ceramics, the lattice distortions are generally caused by dislocations therefore, the strain broadening can be represented and expressed by grain size and dislocation parameters such as concentration, arrangement, etc.,[29].

Some mathematical fitting models were done with data obtained from crystallite size. The best fitting performance was decreasing exponential and its statistical measure for goodness-of-fit, Adj-R square [30], was 96.04%. The mathematical function for this exponential expression is presented in equation 2, and the adjustment of this mathematical model is displayed in fig. 5 a).

$$L_c = 33.932 + 24.389e^{(-t/2.631)} \quad (2)$$

In equation 2, L_c is the crystallite size and "t" is the ball milling time.

Residuals are independent and unbiased [31], because of their randomness (Figure 5 b). Fisher-Test in which the probability P(Fvalue>Ftable) = 2.84638×10^{-6}, lets to conclude that the relationship between experimental and estimated data is statistically significant.

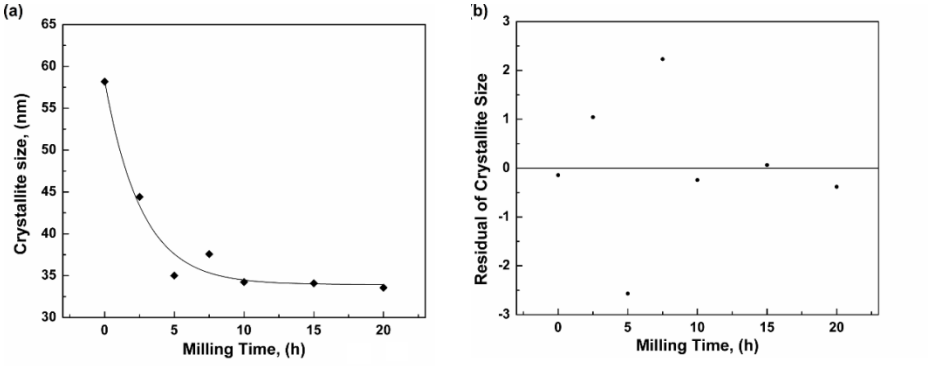

Fig. 5. (a) Crystal size variation of the solid solution Al as a function of processing time, (b) Residuals plot of crystallite size

Crystallite sizes were used to calculate dislocation density. As a first approximation, dislocation density was assumed to be at least one dislocation per crystallite. Hence, according to equation 3, dislocation density (N) becomes the inverse square of the crystallite size (L_c) [32].

$$N = (L_c)^{-2} \tag{3}$$

N: Dislocation density (cm/cm^3); L_c: crystallite size.

Figure 6 a) shows the variation of dislocation density as a function of milling time. This plot exhibits that dislocation density shows a general tendency to increase from beginning to ending of milling process. This comportment is reasonable since multiplication of dislocations is produced by plastic deformation process that occurs during milling. Thus, during deformation process, a hardening of particles is originated by the increment of dislocation density which at the same time promotes fracture of particles and, this is in agreement to the continuous diminution of the size of particles as the milling time had elapsed, see figures 2 and 3.

However, dislocation density decreased from the 5th to the 7.5th hours of ball milling, but after increased again. This behavior could be due to a process of annihilation of dislocations probably induced by a temperature rise as the mechanical alloying process had advanced. Since, it is well known that motion of dislocations may change from conservative to non-conservative or in another words, the climb of dislocations may be induced by an increment of temperature [33]. The process of annihilation of dislocations is typically associated to a recovery process of material being processed. Diminution of dislocations quantity and the rise of crystallite size observed after 5th hours of milling could be related to the temperature rise. In addition, Figures 5 and 6 shows that crystallite size diminished after the 7.5 h but dislocation density exhibited the opposite trend to increase, this couple-phenomena could be associated to the recrystallization process that usually take place after the recovery process [34].

Various mathematical fitting models were adjusted with data corresponding to dislocation density. The best fitting quality for dislocation density factor was of 90.22% [30], through the following exponential function presented in equation 4, and the adjustment of this mathematical model to experimental data is shown in Fig. 6 a).

$$\rho = 8.797x10^{10} - 5.995x10^{10}e^{(-t/4.083)} \tag{4}$$

In equation 4, ρ is the dislocation density (cm/cm^3) and "t" is the processing time.

Residuals are independent and unbiased [31]. Fisher–Test in which the probability $P(F_{value} > F_{table}) = 7.86924x10^{-5}$ is statistically significant. (Figure 6 b)).

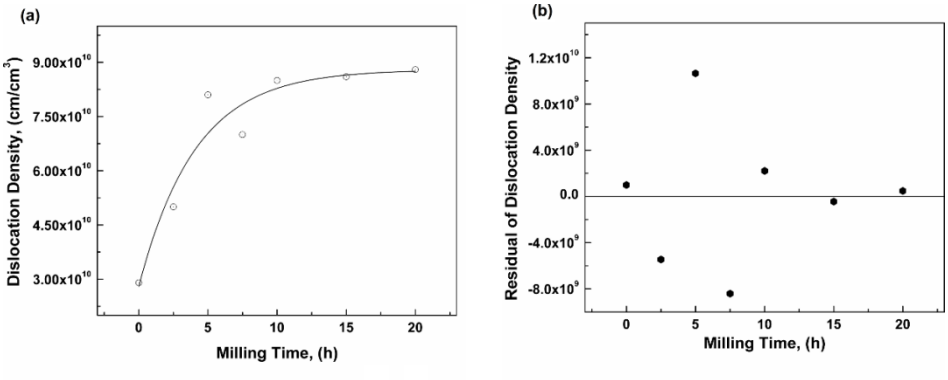

Fig. 6 (a) Variation of dislocation density as a function of milling time, (b) Residuals of dislocation density

Fig. 7 displays reticular constant variation as a function of milling time for Al-3Cu alloy milled at 500 RPM. Change of lattice parameter from 0 to 5 hour of milling exhibits a linear trend, where this behavior is closely related to Law of Vegards. However, figure 7 shows an increment of the reticular lattice after 7.5 hours of processing. This behavior could be ascribed to the size disparity between the solvent (Al) and solute atoms (Cu) which produces the volume change of the solution and, this can be related to the effective lattice parameter [35].

Besides, when variation of reticular constant of the solvent induced by the dissolution of the solute is not linear or deviates from Vegard´s Law, this trend could be due to the fact that the electronic interactions between the outer-most quantum shells of the solute and solvent atoms depend on their electro-chemical nature, reflected in some measure by their positions in the periodic table of elements and, these interactions are far too complex to be considered only by a simple size factor.

A previous research suggested that the trend of a metallic solid solution to deviate from Vegard´s law may actually be interpreted as a measure of the alteration of the electronic environment of the solute atom [36].

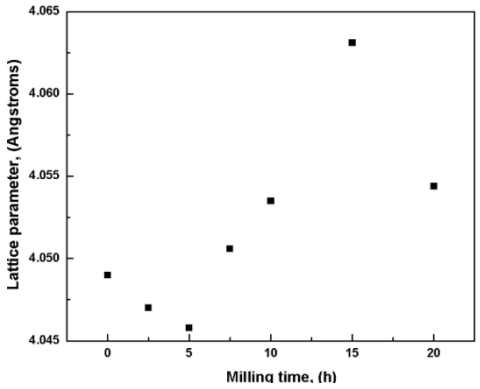

Fig. 7. Variation of the size of lattice parameter of Al-3Cu (wt. %) powder mixture based on milling time

3.3. Microstructural Analysis by SEM of the Aluminum Matrix Nanocomposite.

Fig. 8 shows the microstructure of the powder mixture consisting of a solid solution of composition Al-3Cu (wt. %) which was mixed with 10 and 15 % Vol. TiC. In these micrographs can be observed a homogeneous distribution of the TiC phase into Al-based matrix (brightest particles correspond to the Titanium Carbide). Besides, according to X-Ray chemical mappings, a good distribution of both, Ti and C, into Al-based matrix was detected.

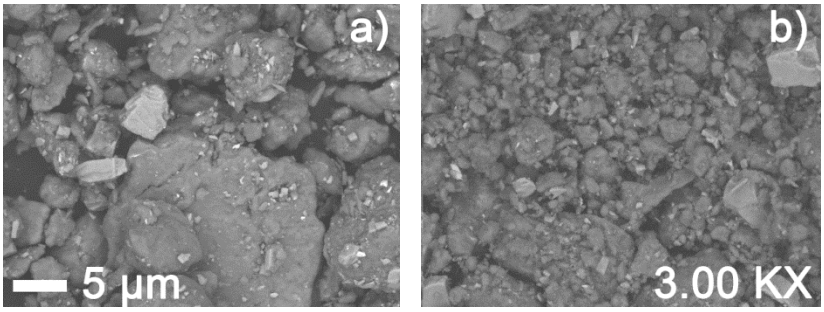

Fig. 8. Secondary electron micrograph of the mixture composed by the powder alloy with composition Al-3Cu (wt. %) with additions of a) 10 % Vol. TiC and b) 15 % Vol. TiC. (after ball milling at 200 RPM during 8 h).

In Figs. 9 and 10, the XRD profiles of Al-3%Cu with 10 % Vol. and 15% Vol. of TiC at different milling times are displayed. In these illustrations, the absence of Cu peaks is observed, this finding is related to the achievement of a complete solubility of copper in the aluminum solvent. Also, the TiC diffraction peaks do not exhibit a significant variation in the width of peak and, also in its intensity. Diffraction peaks of very low intensity corresponding to the Al_2CuO_4 phase is exhibited in the same XRD spectrums, formation of this oxide is due to a possible oxidation process that could have been developed during the mechanical milling. In addition, the existence of C revealed in these X-Ray diffraction profiles could have been formed by the reaction represented in equation 5.

$$TiC_{(s)} \rightarrow Ti_{(s)} + C_{(s)} \tag{5}$$

Equation 5 indicates that during the milling process, thermodynamic conditions were reached in order to induce the dissociation of Titanium Carbide. Also, another possible cause for the presence of carbon, could be due to the provision of this element by the Process Control Agent (PCA).

Besides, the absence of diffraction peaks corresponding to the formation of second phases different from α-Al and TiC, suggest that mechanochemical reactions between α-Al and TiC were not induced during the ball milling process. Also, the highest intensity peaks corresponding to α-Al displayed a broadening tendency which is related to a diminution of crystallite size [25].

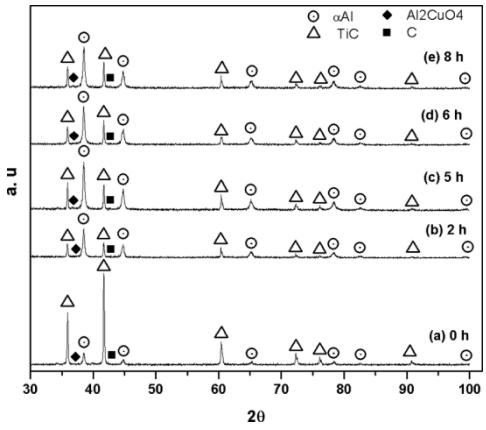

Fig. 9. X-Ray diffraction patterns of Al-3Cu (wt. %) powder mixture with addition of 10 % Vol. TiC milled at 200 RPM at various times: a) 0 h, b) 2 h, c) 4 h, d) 6 h and e) 8 h.

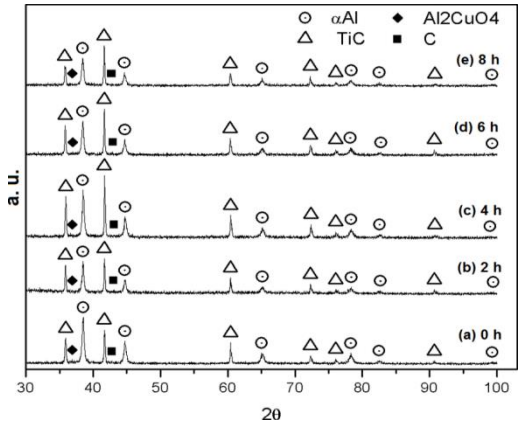

Fig. 10 X-Ray diffraction patterns of Al-3Cu (wt. %) powder mixture with addition of 15 % Vol. TiC milled at 200 RPM at various times: a) 0 h, b) 2 h, c) 4 h, d) 6 h and e) 8 h

Fig. 11 displays the lattice parameter evolution of the Al-3Cu alloy with 10 % Vol. and 15 % Vol. of TiC. In this plot, reticular constant showed a tendency to increase while milling time had elapsed, this behavior that does not correlates to that described by the Vegard´s Law could be the result of various factors, including the super saturation of Cu in Al, an increase in lattice distortion, possible dissociation of TiC (see equation 5) and interstitial solution of carbon inside the Al-based matrix. In addition, previous investigations have reported formation of carbon clusters inside the Al lattice [37, 38]. Reticular constant of α-Al of the specimen with higher reinforcement content displayed an initial rapid trend to rise during the first 4 hours of milling; however, after 4 hours, lattice constant variation exhibited an asymptotic behavior. This comportment is the result of the transfer of a higher mechanical energy provided to the metal-ceramic system caused from a higher TiC content. In this case, these hard ceramic particles acted as milling media which induced that lattice parameter had reached a limit in less time than the alloy with less TiC content. Further refinement of crystallite than the one obtained after 20h of milling for the solid solution (Al-α) was achieved by the addition of TiC particles. Nonetheless, figure 12 displays a greater crystallite refinement in the sample with 15 % vol. of TiC than the specimen reinforced with 10 % vol. of TiC, meanwhile, the crystallite size of the specimen with 10 % vol. TiC displays an asymptotic behavior after the 4th hour of process. This behavior means that minimum crystallite size was going to be reached under these milling conditions which is associated with a balance between welding and fracture of particles. However, when TiC phase was added in a quantity of 15 % vol., crystallite size of (Al-α) exhibited a trend to decrease even up to the 20th hour of milling.

Different mathematical fitting models were adjusted to the data corresponding to lattice parameter for Al-3Cu alloy with additions of 15 % vol. TiC.

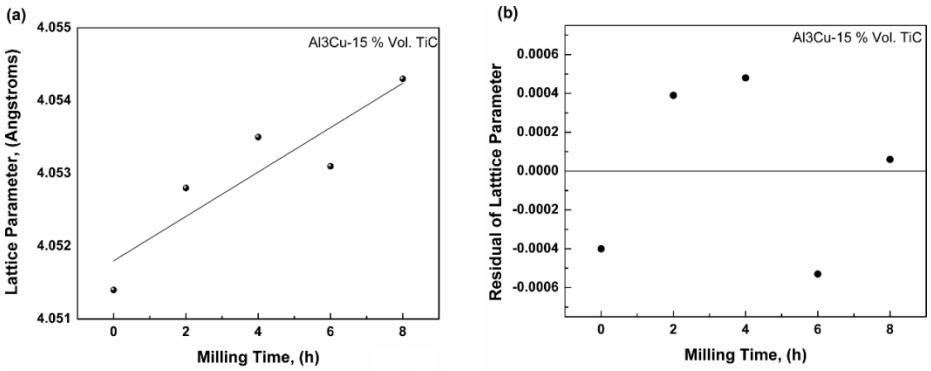

Fig. 11. (a) Lattice parameter dependence with milling time of alloys Al-3%Cu with addition of 15% Vol. de TiC, (b) Residuals of lattice parameter

The best fitting quality for lattice parameter (∝-Al-15Vol%TiC) data was of 75.755% [30], through the linear function presented in equation 6. And the linear adjustment to the experimental data is displayed in Figure 11 a).

$$a = 4.0518 + 3.05x10^{-4}t \quad (6)$$

In equation (6) "a" is the lattice parameter, "t" is de milling time.

In this case, the residuals are independent and unbiased [31]. Fisher-Test in which the probability P(Fvalue>Ftable) = 0.0349 is statistically significant (Fig. 11 b)).

In the same way, various mathematical fitting models were adjusted to the experimental data corresponding to lattice parameter for Al-3Cu alloy with additions of 10 % Vol. TiC.

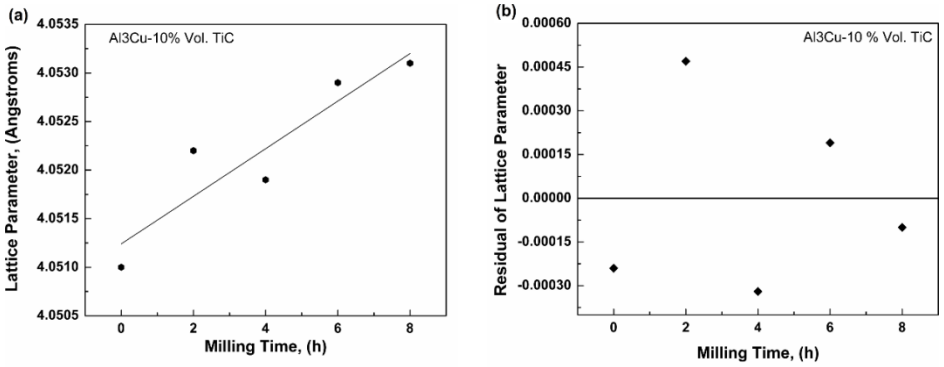

Fig. 12. (a) Lattice parameter dependence with milling time of alloys Al-3%Cu with addition of 10% Vol. de TiC, (b) Residuals of lattice parameter

The best fitting performance for the lattice parameter data of Al3Cu-10%Vol. TiC was a value of 79.868%, through the linear function presented in equation 7 as follows:

$$a = 4.0512 + 2.45\ x\ 10^{-4}t \quad (7)$$

In the previous equation "a" is the lattice parameter and "t" is the processing time.

Similarly, various mathematical fitting models were fitted to the experimental data corresponding to crystallite size for Al-3Cu alloy with additions of 15 % Vol. TiC.

The best fitting performance in this case was a decreasing exponential function and its statistical measure for goodness-of-fit, Adj-R square was 97.202% [30]. In this case, the exponential fitting to the experimental data is presented in Figure 13 a).

The mathematical function for this exponential expression is presented in equation 8 as follows:

$$L_c = 16.87174 + 4.49224\ e^{-t/7.92922} \quad (8)$$

In the anterior equation L_c is the crystallite size, "t" is the milling time.

Residuals are independent and unbiased [31], because of their randomness (Fig. 12 b)). Fisher-Test in which the probability $P(F_{value}>F_{table})$ = 5.58797 x 10^{-5}, lets to conclude that the relationship between experimental and estimated data is statistically significant.

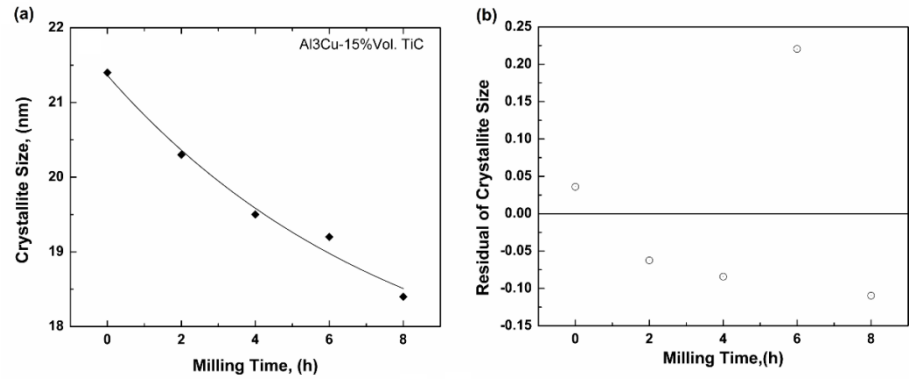

Fig. 13. (a) Crystallite size dependence as a function of milling time for the alloy Al-3Cu with addition of 10%Vol. TiC, (b) Residuals of crystallite size

The best fitting conduct for α – Al – 10 Vol. %TiC was a Boltzmann function and its statistical measure for goodness-of-fit, Adj-R square was 99.85% [30]. The fitting of the Boltzmann model to the experimental data is displayed in Fig. 14 a). The mathematical function for this Boltzmann expression is presented in equation 9 as follows:

$$L_c = \frac{(22.61149-17.33612)}{1+e^{(t-2.76996)/dt}} + 17.33612 \quad (9)$$

In equation 9, L_c is the crystallite size and "t" is the milling time.

In this case, residuals are independent and unbiased [31], because of their randomness. Fisher-Test in which the probability P (F_{value}>F_{table}) = 0.00181, lets to conclude that the relationship between experimental and estimated data is statistically significant, see fig. 14 b).

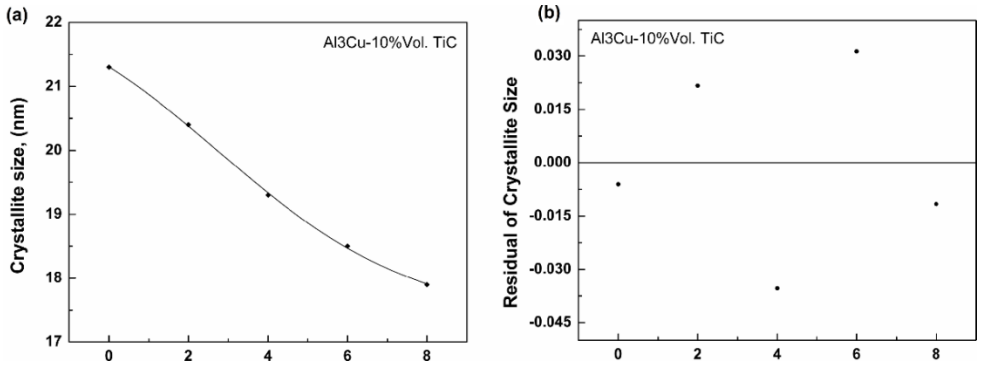

Fig. 14. Crystallite size dependence as a function of milling time for the Al-3Cu alloy with addition of 10 % Vol. TiC

4. Conclusions

In the first stage of mechanical alloying process, the particle size of the initial powder mixture of composition Al-3%wt.Cu decreased as the milling time had advanced from the beginning to the end of processing. According to the X-Ray Diffraction Analysis, a solid solution of Cu in Al was formed at the 10th. The crystallite size pertaining to the solid solution of Cu in Al (α-Al), decreased from 55 nm to 33 nm as the milling time elapsed from 2.5 to 20 h.

Constant reduction of the crystallite size was explained in terms of generation of crystallographic defects of linear type since, when a certain quantity of dislocation density is achieved, within specific heavily strained regions. Then, the crystal decompose into subgrains

which are initially separated by low-angle grain boundaries and, the continuous formation of subgrains is related to the reduction of crystallite size.

The computation of lattice strain denoted an accelerated initial energy storage in the powder mixture as a consequence of the rapid generation of crystallographic defects in the material, however, after the 5th hour of milling, a recovery process takes place. This phenomenom probably occurred by the temperature rise that occurs during the process of mechanical milling.

Lattice parameter of Al-α solid solution change in a linear way while milling time had elapsed from 0 to 5 h of milling. In this case, lattice parameter follow the Law of Vegard. However, after the 5th h of milling, reticular constant exhibited a deviation from the Law of Vegard. This behavior could be explained as a measure of the modification of the electronic environment of the solute atom (Cu).

During mechanical milling stage, the powder mixture composed by the solid solution Al-α together with the TiC did not experienced a mechanochemical reaction that could give place to the formation of second phases. This un-reactivity of metal with ceramic phase could be due to the fact that the ball milling was performed under low energy conditions.

During the ball milling process of the powder mixture composed by the solid solution Al-α together with the TiC, a further reduction of the crystallite size of the Al-α phase was observed, where this behavior is associated to the fact that the ceramic TiC particles acted as milling media.

Acknowledgements

The authors express their gratitude to Prodep-Sep México for the financial support granted for the development of the project UPMOR-PTC-046 that provided the results presented in this article. Also to the technician Adriana Tejeda for the realization of the X-Ray diffraction analyses.

References

[1] A. A. Karimpoor, U. Erb, K.T. Aust, G. Palumbo, Scripta Mater **49**, 651 (2003).
[2] C. Granqvist, L. Kish, W Marlow, Gas Phase Nanoparticle Synthesis, Kluwer Academic, Dordrecht, The Netherlands (2004).
[3] H.S Nalwa, Handbook of Nanostructured Materials and Nanotechnology, Vol. I: Synthesis and Processing, Academic Press, San Diego, CA (2000).
[4] C. Suryanarayana, Progress in Materials Science **46**, 1 (2001).
[5] C. Suryanarayana, Mechanical Alloying and Milling, Marcel Dekker, New York, NY (2004).
[6] R.Z. Valiev, R.K. Islamgaliev, I.V. Alexndrov, Progress in materials science **45**, 103 (2000).
[7] N. A. Smirnova, V. I. Levit, V. I. Pilyugin, R. I Kuznetsov, L. S. Davydova, V. A. Sazonova, Fiz. Met. Metalloved **68**, 1170 (1986).
[8] V. M. Segal, Materials Science & Engineering **A197**, 157 (1995).
[9] Y. Saito, N. Tsuji, H. Utsunomiya, T. Sakai, R.G. Hong, Scripta Materiala **39**, 1221 (1998).
[10] J. S. Benjamin, Metallurgical Transactions **A1**, 2943 (1970).
[11] C. Suryanarayana, F.H. Froes, Nanostructured Materials **3**,147 (1993).
[12] J. Naser, W. Reinhemann, H. Ferkel, Materials Science & Engineering **A234**, 467 (1997).
[13] P. Matteazzi, G. L. Caër, Journal of the American Ceramic Society **75(**10), 2749 (1992).
[14] P. Matteazzi, G. Le Caër, Journal of alloys and compounds **187**(2), 305 (1992).
[15] M. Khakbiz, F. Akhlaghi, Journal of Alloys and Compounds **479**, 334, (2009).
[16] J. B. Correia, M. T. Marques, P. A. Carvalho, R. Vilar, Journal of Alloys Compounds **434**, 301 (2007).
[17] Z. G. Huang, Z. P. Guo, A. Calka, D. Wexler, H. K. Liu, Journal of Alloys Compounds **427**, 94 (2007).
[18] R. Vijay, R. Sundaresan, M. P. Maiya, S. Srinivasa Murthy, Journal of Alloys Compounds **424**, 289 (2006).
[19] F. Karimzadeh, M.H. Enayati, M. Tavoosi, Materials Science & Engineering A **486**, 45 (2008).

[20] K. H. Chung, J. He, D. H. Shin, J. M. Schoenung, Materials Science & Engineering A **356**, 23 (2003).
[21] J. Li, X. Ni, G. Wang, Journal of Alloys and Compounds **44**, 349 (2007).
[22] J. L. Bobet, C. Even, Y. Nakamura, E. Akiba, B, Darriet, Journal of Alloys and Compounds, **298**(1), 279 (2000).
[23] J. B. Fogagnolo, E. M. Ruiz-Navas, M. H. Robert, J. M. Torralba, Materials Science & Engineering A, **355**(1), 50 (2003).
[24] J. B. Fogagnolo, M. H. Robert, J. M. Torralba, Materials Science &Engineering A, **426**(1), 85 (2006).
[25] A. Monshi, M. R. Foroughi, M. R. Monshi, World Journal of Nano Science and Engineering, **2**(03), 154 (2012).
[26] Y. T. Prabhu, K. V. Rao, V. S. S. Kumar, B. S Kumari, World Journal of Nano Science and Engineering **4**(01), 21 (2014).
[27] V. D. Mote, Y. Purushotham, B. N. Dole, Journal of Theoretical and Applied Physics **6**(1), 1 (2012).
[28] E. Hellstern, H.J. Fecht, C. Garland, W.L. Johnson, presented at the MRS Symp. Proc. **132,** 137 (1989).
[29] Y. Saberi, S. M. Zebarjad & G. H. Akbari Journal of Alloys and Compounds **484**(1), 637 (2009).
[30] G. D. Garson, "Curve Fitting & Nonlinear Regression", North Carolina State University, Statistical Associates, Publishing Blue Book Series, 2012.
[31] G. D. Garson, "Testing Statistical Assumptions", North Carolina State University, Statistical Associates, Publishing Blue Book Series, 2012.
[32] T. Raghu, R. Sundaresan, P. Ramakrishnan & T. R. Mohan, Materials Science and Engineering A **304**, 438 (2001).
[33] D.Hull D. J. Bacon, Introduction to dislocations. Butterworth-Heinemann, Oxford (2001).
[34] A. Rollett, F. J. Humphreys, G. S. Rohrer, M. Hatherly, Recrystallization and related annealing phenomena, Elsevier, Amsterdam (2004).
[35] V. A. Lubarda, Mechanics of Materials, **35**(1), 53 (2003).
[36] H.W. King, Journal of Materials Science **1**, 79 (1966).
[37] M.T. Marques, J.B. Correia, O. Conde, Scripta Materiala 50, 963 (2004).
[38] L. Xueran, L. Yongbing, R. Xu, A. Jian, C. Zhanyi, Materials Characterization V. **58**(I 6), 504 (2007).